



# A beryllium-10 chronology of late-glacial moraines in the upper Rakaia valley, Southern Alps, New Zealand supports Southern-Hemisphere warming during the Younger Dryas



Tobias N.B. Koffman <sup>a</sup>, Joerg M. Schaefer <sup>a,b</sup>, Aaron E. Putnam <sup>a,c,\*</sup>, George H. Denton <sup>a,c</sup>, David J.A. Barrell <sup>d</sup>, Ann V. Rowan <sup>e</sup>, Robert C. Finkel <sup>f</sup>, Dylan H. Rood <sup>g,h</sup>, Roseanne Schwartz <sup>a</sup>, Mitchell A. Plummer <sup>i</sup>, Simon H. Brocklehurst <sup>j</sup>

<sup>a</sup> Lamont–Doherty Earth Observatory of Columbia University, 61 Rt. 9W, Palisades, NY 10964, USA

<sup>b</sup> Department of Earth and Environmental Sciences, Columbia University, New York, NY 10027, USA

<sup>c</sup> School of Earth and Climate Sciences and Climate Change Institute, University of Maine, Orono, ME 04469, USA

<sup>d</sup> GNS Science, Private Bag 1930, Dunedin 9054, New Zealand

<sup>e</sup> Department of Geography, University of Sheffield, Sheffield, S10 2TN, UK

<sup>f</sup> Department of Earth and Planetary Sciences, University of California, Berkeley, CA 95064, USA

<sup>g</sup> Department of Earth Science & Engineering, Imperial College London, South Kensington Campus, London SW7 2AZ, UK

<sup>h</sup> Center for Accelerator Mass Spectrometry, Lawrence Livermore National Laboratory, Livermore, CA 94550, USA

<sup>i</sup> Idaho National Laboratory, Idaho Falls, ID 83415-2107, USA

<sup>j</sup> School of Earth and Environmental Sciences, University of Manchester, Manchester M139PL, UK

## ARTICLE INFO

### Article history:

Received 6 February 2017

Received in revised form

5 June 2017

Accepted 13 June 2017

### Keywords:

Pleistocene

Holocene

Paleoclimatology

Glaciology

Southern Pacific

Cosmogenic isotopes

Glacial geomorphology

Glaciological modeling

## ABSTRACT

Interhemispheric differences in the timing of pauses or reversals in the temperature rise at the end of the last ice age can help to clarify the mechanisms that influence glacial terminations. Our beryllium-10 (<sup>10</sup>Be) surface-exposure chronology for the moraines of the upper Rakaia valley of New Zealand's Southern Alps, combined with glaciological modeling, show that late-glacial temperature change in the atmosphere over the Southern Alps exhibited an Antarctic-like pattern. During the Antarctic Cold Reversal, the upper Rakaia glacier built two well-defined, closely-spaced moraines on Reischek knob at  $13,900 \pm 120$  [ $1\sigma$ ;  $\pm 310$  yrs when including a 2.1% production-rate (PR) uncertainty] and  $13,140 \pm 250$  ( $\pm 370$ ) yrs ago, in positions consistent with mean annual temperature approximately 2 °C cooler than modern values. The formation of distinct, widely-spaced moraines at  $12,140 \pm 200$  ( $\pm 320$ ) and  $11,620 \pm 160$  ( $\pm 290$ ) yrs ago on Meins Knob, 2 km up-valley from the Reischek knob moraines, indicates that the glacier thinned by ~250 m during Heinrich Stadial 0 (HS 0, coeval with the Younger Dryas 12,900 to 11,600 yrs ago). The glacier-inferred temperature rise in the upper Rakaia valley during HS 0 was about 1 °C. Because a similar pattern is documented by well-dated glacial geomorphologic records from the Andes of South America, the implication is that this late-glacial atmospheric climate signal extended from 79°S north to at least 36°S, and thus was a major feature of Southern Hemisphere paleoclimate during the last glacial termination.

© 2017 Elsevier Ltd. All rights reserved.

## 1. Introduction

The last glacial termination is a key interval for understanding the role of millennial-scale climate events in ice-age climate cycles. In seeking to determine the causes and effects of the Antarctic Cold

Reversal (ACR) and Heinrich Stadial 1 and 0 (HS 1, HS 0; the latter equating to the Younger Dryas), we must first understand their timings and geographic footprints. Isotope records from Antarctic ice cores indicate cooling during the ACR followed by renewed warming during HS 0 (Brook et al., 2005; Stenni et al., 2011; Pedro et al., 2011; WAIS Divide Project Members, 2013; Buizert et al., 2015; Cuffey et al., 2016). Greenland ice cores show nearly opposite isotopic patterns (e.g., Rasmussen et al., 2006). However, these antiphased changes in the polar latitudes of both hemispheres are of uncertain geographic extent, making it difficult to ascertain their

\* Corresponding author. Lamont–Doherty Earth Observatory of Columbia University, 61 Rt. 9W, Palisades, NY 10964, USA.

E-mail address: [aaron.putnam@maine.edu](mailto:aaron.putnam@maine.edu) (A.E. Putnam).

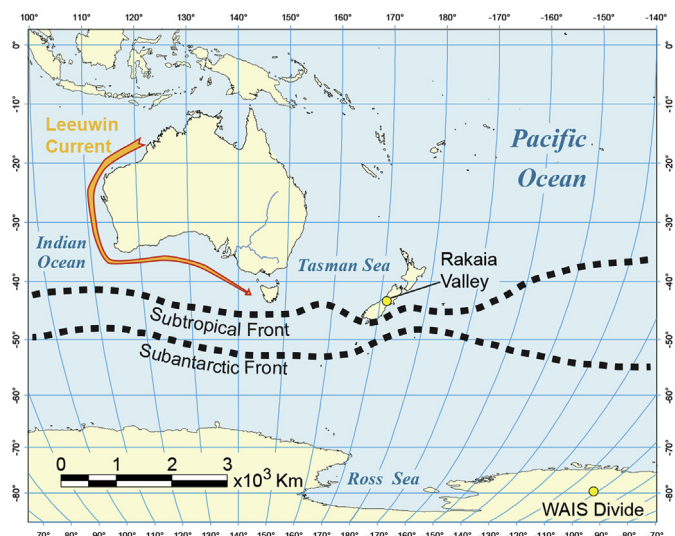


**Fig. 1.** Map of a portion of the Southern Hemisphere including New Zealand, Australia, and part of Antarctica. Ocean current depictions adapted from Carter et al. (1998) and Orsi et al. (1995).

causes as well as their potential significance in regard to the behavior of Earth's climate system. For example, to what extent did the Antarctic pattern impinge on the Southern Hemisphere's mid-latitudes (Newnham et al., 2012; Pedro et al., 2016)? Glacial landforms in New Zealand's Southern Alps provide archives suitable for ascertaining the timing of climate warming during the last glacial termination, and thereby test hypotheses about the geographic footprints of regional to hemispheric climate events. Here, we present a chronology of late-glacial moraine formation in the upper reaches of the Rakaia valley. Our dataset complements the chronology of ice recession during the last glacial termination obtained by dating of glacial landforms farther down the Rakaia valley (Putnam et al., 2013b). The quantification of glacier recession in a single valley in the Southern Alps reduces possible concerns about valley-specific differences in glacier behavior arising from factors such as topography, aspect and geometry. The Southern Alps are situated near the antipode of the North Atlantic region, and thus are aptly positioned to test the inter-hemispheric phasing of millennial-scale climate changes. Furthermore, the Southern Alps lie athwart the Southern Hemisphere westerly winds at the northern edge of the Southern Ocean, marked by the Subtropical Front (STF, Fig. 1; Bostock et al., 2015). Their location near the STF makes the Southern Alps subject to both tropical and Antarctic influences (De Deckker et al., 2012; Putnam et al., 2012, 2013a). Variations in present-day glacier mass balance in the Southern Alps are largely attributed to changes in air temperature, due both to solar radiation and to turbulent heat flux from air masses passing over the ocean west of New Zealand; precipitation changes play a lesser role (Anderson and Mackintosh, 2006). Consequently, length variations of glaciers in New Zealand's Southern Alps can be linked primarily to changes in air temperature (Oerlemans, 1997, 2005; Anderson and Mackintosh, 2006; Anderson et al., 2010; Purdie et al., 2011; Gollidge et al., 2012). This provides a basis for inferring that glacial landforms in the Southern Alps (Fig. 2) document times of greater-than-present ice extent that resulted primarily from atmospheric temperatures that were colder than present.

The Rakaia valley glacial landforms record progressive ice recession during the last glacial termination (Fig. 3) (Burrows and Russell, 1975; Shulmeister et al., 2010; Barrell, 2011; Barrell et al., 2011; Putnam et al., 2013b). A notable feature is that the lower

reaches of the Rakaia valley occupy a tectonic depression, rather than being of purely ice-hewn origin (Barrell et al., 2011). Consequently, there is not a well-defined glacial trough. In addition, numerous, glacially-sculpted bedrock hills and spurs project from the valley floor and walls. Glacially-transported boulders on both the ice-sculpted rock surfaces and the morainic deposits afford opportunities for palaeoclimatic investigation (Putnam et al., 2013b). Using mapped glacial landforms as targets (Barrell et al., 2011), we employed  $^{10}\text{Be}$  surface-exposure dating and glaciological modeling in the upper reaches of the Rakaia valley to reconstruct a chronology of ice extent and associated climate during the latter part of the last glacial termination. Our work builds upon the chronology of Putnam et al. (2013b), which shows the details of ice retreat during the first part of the last glacial termination in the Rakaia valley from ~18,000 to ~15,000 years ago. On the basis of our mapping, surface-exposure dating, and climate reconstruction, we discuss the climate events of the last glacial termination in the Southern Alps.

## 2. Geology and geomorphology of the upper Rakaia valley

The Rakaia valley drains a portion of the southeast side of the main hydrographic divide (Main Divide) of the Southern Alps. During the Last Glacial Maximum (LGM) the former Rakaia glacier was a major outlet of the Southern Alps ice field (Barrell et al., 2011). Bedrock in the Rakaia catchment comprises predominantly greywacke sandstone and argillite mudstone of the Rakaia Terrane (Cox and Barrell, 2007). The Rakaia valley is fed by three major tributaries, from north to south, the Wilberforce River, the Mathias River, and the upstream reach of the Rakaia River, hereafter the upper Rakaia River, which flows down the upper Rakaia valley (Fig. 3). The upper Rakaia River has its source at the confluence of the meltwater streams from the Lyell Glacier and the Ramsay Glacier. Although aggradation of the upper Rakaia valley floor, and gully erosion of the valley sides, have obscured or removed much of the glacial imprint in the upper Rakaia valley, important remnants of moraines persist, particularly on the crests and flanks of ice-smoothed bedrock spurs (Barrell et al., 2011). On the eastern flank of Reischek Stream, morainial landforms occupy the northern and western flanks of a bedrock spur. The spur was referred to as "high moraine bluff" by Burrows and Russell (1975) and as "Reischek knob" by Putnam et al. (2013b). The Reischek knob moraines were formed at the margin of a much-expanded Reischek Glacier, at a time when it was confluent with the upper Rakaia glacier, itself the product of the much-expanded and coalesced Lyell and Ramsay glaciers. Burrows and Russell (1975) tentatively correlated the higher and lower portions of a prominent moraine ridge complex on Reischek knob with glacier termini near Lake Stream (higher ridge) and Jagged Stream (lower ridge), respectively ~17 km and ~11 km down-valley of Reischek knob. Standing on the southern side of the confluence of the Lyell and Ramsay valleys is Meins Knob, a broad-crested bedrock ridge, capped with remnant glacial landforms (Meins Knob moraines of Burrows and Russell (1975)). As Meins Knob lies ~2 km up-valley, and as much as 200 m elevation lower than, the prominent moraine ridges on Reischek knob, the Meins Knob moraines were formed after the upper Rakaia glacier had attained a lesser elevation than it had at the time the Reischek knob moraines were formed.

A recent study documented the geomorphology and moraine chronology of the Rakaia valley from Reischek knob downstream (Putnam et al., 2013b). That study examined two landform features on Reischek knob, outboard of the prominent moraine ridges on the knob. Those landform features were given informal names and comprise till-veneered bedrock (Reischek knob I), and meltwater channels incised into, and therefore younger than, the till-veneered

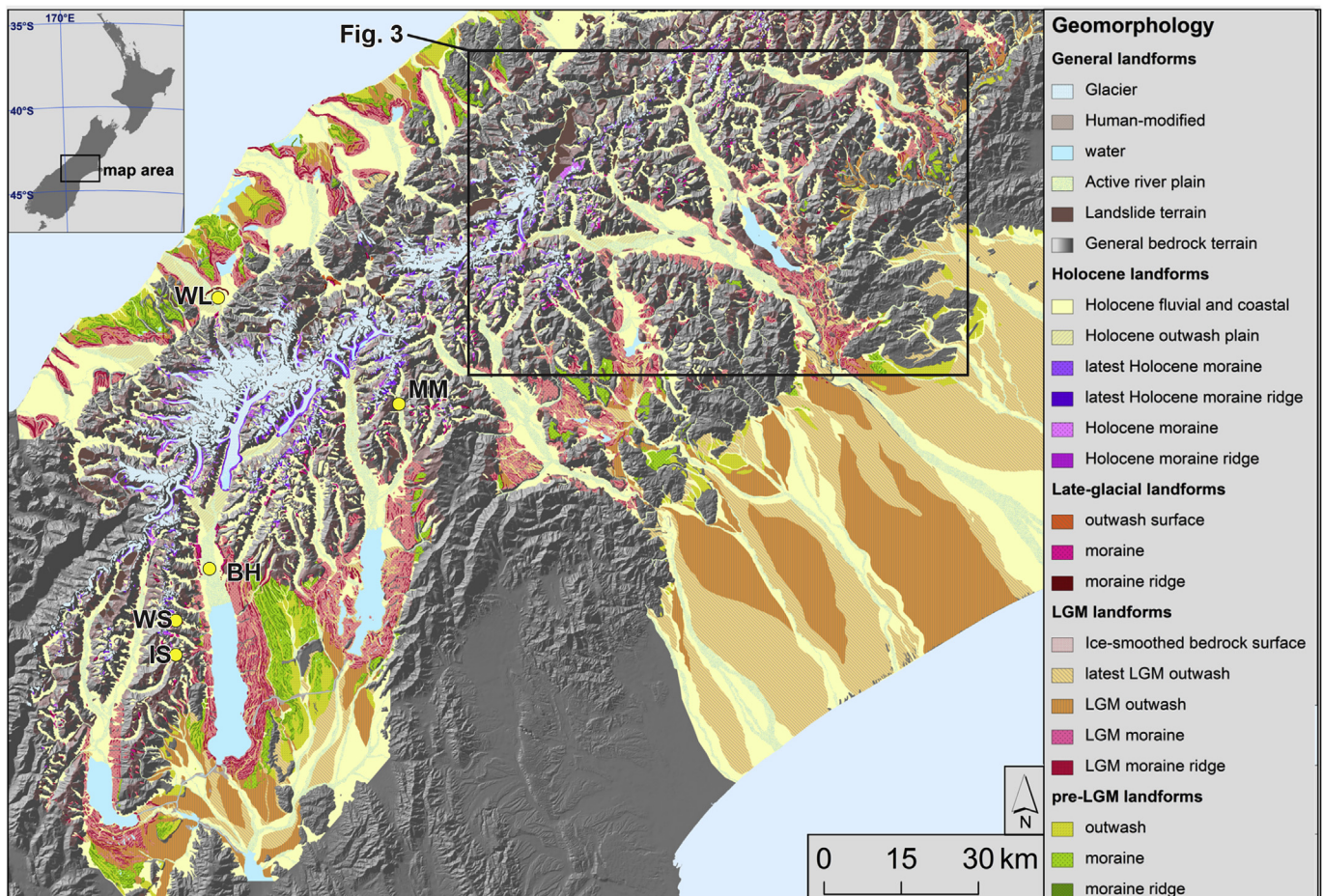


**Fig. 2.** Glacial geomorphologic map of the central South Island of New Zealand, adapted by Putnam et al. (2013b) from Barrell et al. (2011). Rakaia valley study area outlined in black box appears in more detail in Fig. 3. Abbreviations of moraine locations mentioned in the text are: BH, Birch Hill; IS, Irishman Stream; MM, middle Macaulay valley; WL, Waiho Loop; WS, Whale Stream. Geomorphic symbols explained in the legend apply also to Fig. 3.

bedrock landform (Reischek knob II). The meltwater channels emanate from the outermost part of the moraine ridge complex. The study area adjoins that of Putnam et al. (2013b) and the oldest landforms addressed in our study are in the moraine ridge complex on Reischek knob. Within the moraine ridge complex, we focused on two prominent moraine ridges, the outer (higher) identified here as Reischek III, and the inner (lower) as Reischek IV.

The moraines on Meins Knob follow the long axis of this bedrock spur, which is nearly perpendicular to the trend of the Rakaia valley (see map, Fig. 4). The Meins Knob I moraine extends ~1200 m along the top of the spur. The Meins Knob II moraine ridge extends ~500 m along the western slope of the spur, and lies ~200 m up-valley from, and ~100 m lower than, the Meins Knob I moraine ridge. Between these two moraine ridges is a flight of low ridges or kame terraces, each of which lacks surface boulders.

### 3. Methods

#### 3.1. Sampling for $^{10}\text{Be}$ surface-exposure dating

We used  $^{10}\text{Be}$  surface-exposure dating to build a chronology of the Reischek knob III and IV moraines and the Meins Knob moraines. We selected for sampling boulders that were well embedded in moraine ridges. We avoided sampling boulders on portions of moraines that showed signs of post-depositional disturbance such as erosion or slumping, and boulders on

landforms situated below cliffs and steep slopes that could have been emplaced by rock fall subsequent to ice withdrawal. We also avoided boulders that showed signs of surface instability such as spalling or flaking. We used a hammer and chisel, or else the drill-and-blast method of Kelly (2003), to sample the top one-to-five cm of boulders that were deemed suitable for dating.

#### 3.2. Laboratory procedures and $^{10}\text{Be}$ age calculations

We processed all samples for  $^{10}\text{Be}$  analysis at the Lamont-Doherty Earth Observatory cosmogenic isotope laboratory, following the methods described by Schaefer et al. (2009), and available online at <http://www.ldeo.columbia.edu/tcn>. The LDEO cation exchange column that we used to separate Be from Ti and Al generally follows the procedure adapted by Stone ([http://depts.washington.edu/cosmolab/chem/Al-26\\_Be-10.pdf](http://depts.washington.edu/cosmolab/chem/Al-26_Be-10.pdf)) from that of Ditchburn and Whitehead (1994). Beryllium isotope ratios were measured at the Lawrence Livermore National Laboratory Center for Accelerator Mass Spectrometry (Rood et al., 2010, 2013). We corrected sample  $^{10}\text{Be}$  quantities ( $1.6\text{--}3.2 \times 10^5$  atoms  $^{10}\text{Be}$ ) for background  $^{10}\text{Be}$  contamination by subtracting the total number of  $^{10}\text{Be}$  atoms measured in one or two procedural blanks ( $0.1\text{--}1.4 \times 10^4$  atoms  $^{10}\text{Be}$ , see Table 3) that were run with each respective sample, and propagated sample and blank uncertainties in quadrature, including a 1.5% uncertainty in the  $^9\text{Be}$  carrier concentration. In cases where two blanks were run with a sample, we

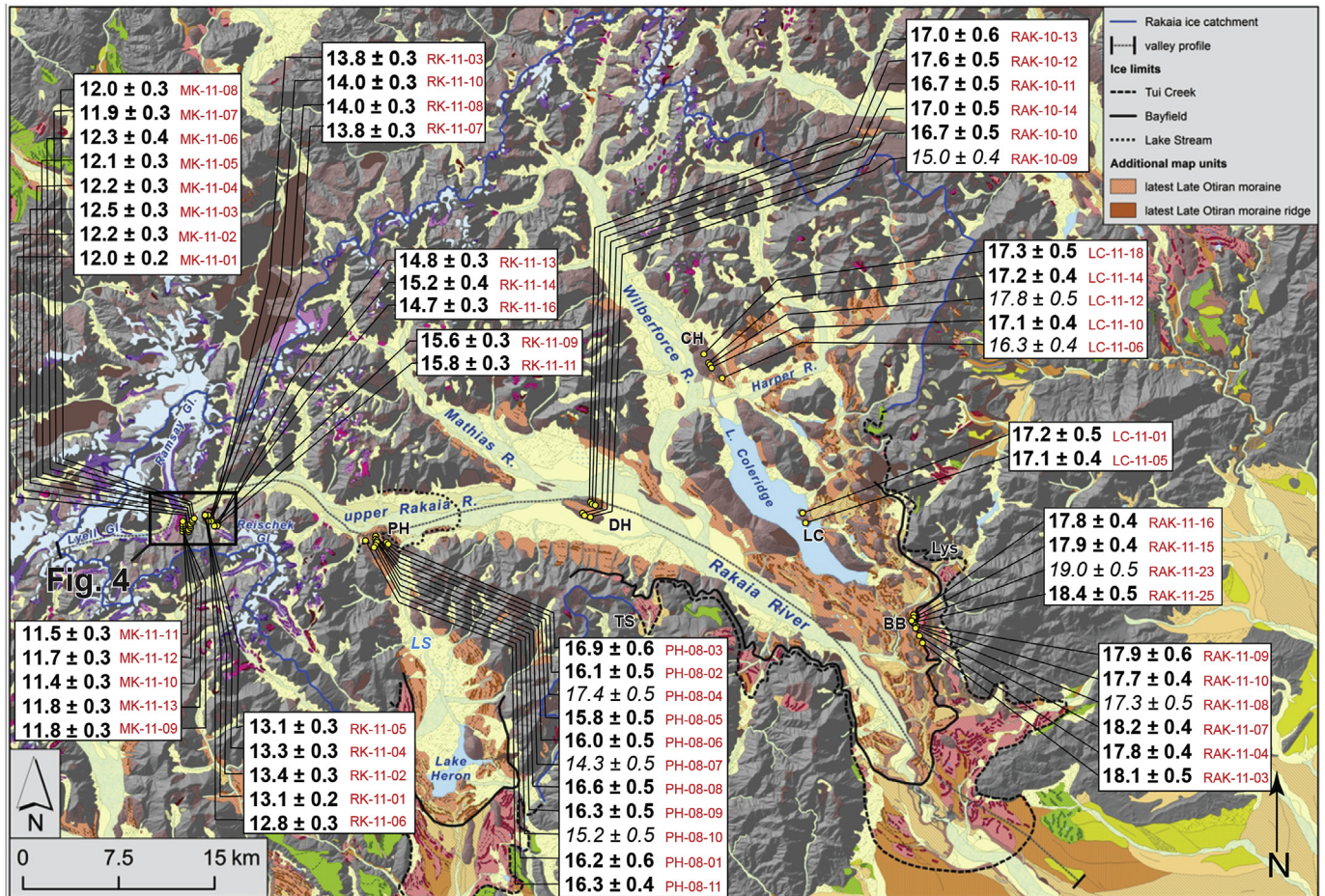


**Fig. 3.** Glacial geomorphologic map of the Rakaia valley after Barrell et al. (2011).  $^{10}\text{Be}$  ages of late-glacial landforms on Reischek knob and Meins Knob, located near the western headwaters of the valley, are shown in more detail in Fig. 4. Dates showing glacier retreat during HS1 (Putnam et al., 2013b) are shown for context; outliers omitted from mean landform ages are shown in italic print. Geographic abbreviations are: BB, Big Ben; CH, Castle Hill; DH, Double Hill; LC, Lake Coleridge; LyS, Lyndon saddle; PH, Prospect Hill; TS, Turtons Saddle. All ages are shown with  $1\sigma$  analytical error (internal error only) to facilitate comparison within the Rakaia valley. Valley profile is shown in Fig. 6.

used the average and standard deviation of both blanks. Background  $^{10}\text{Be}/^9\text{Be}$  ratios were less than one percent of sample  $^{10}\text{Be}/^9\text{Be}$  ratios (Table 1); uncertainty in the background corrections affects the overall age uncertainty by less than 0.2%.

We determined exposure ages by using the online calculator of Balco et al. (2008) with the production-rate calibration data of Putnam et al. (2010a), which imply  $^{10}\text{Be}$  production of  $3.74 \pm 0.08$  at  $\text{g}^{-1} \text{yr}^{-1}$  at sea level and high latitude (with the time-dependent scaling scheme of Lal (1991)/Stone (2000) ("Lm")). Ages given in the text were calculated using Lm scaling (Table 2) that includes the high-resolution geomagnetic model of Lifton et al. (2008). Because the Macaulay River calibration site of Putnam et al. (2010a) is located about 40 km southwest of the upper Rakaia valley and lies at a similar elevation, the choice of scaling scheme has little impact on the exposure ages (see Table 2).

We made no corrections for snow cover or for erosion of boulder surfaces. In the central part of the Southern Alps, winter (June–July–August) snow cover is generally persistent only at altitudes above ~1500 m. Below that altitude a winter snowfall of 1 m is an exceptional event and generally melts away within a few weeks. Moreover, the sampled boulders protrude from the crests of moraine ridges and are likely to be swept clear of snow by the wind. Thus, at the elevation of our sample sites (1150–1450 m above sea level), significant shielding due to snow is unlikely, especially given the northerly (sunny) aspect of Reischek knob and Meins Knob.

Quartz veins that protrude 2–10 mm from the surface of many of the sampled boulders indicate low erosion rates of 0.2–0.7 mm/ka. Assuming erosion of 0.7 mm/ka would make the ages some 0.6–0.7% older. We chose not to make any erosion corrections for several reasons. One is that quartz-vein heights, and thus the implied erosion rates, vary from one boulder to another. Another is that at the production-rate calibration site no erosion correction was applied, and so the effects, if any, of erosion are integrated within the production rate. Finally, the effect on the calculated ages of an erosion correction would in any case be minimal. Another consideration is the question of pre-exposure, which may result in inherited  $^{10}\text{Be}$  concentrations. Rapid erosion and frequent rock fall in the steep glacier catchments of the Southern Alps means that in general the rock wall surfaces of the valleys are regularly being refreshed. Thus, the material delivered to the glaciers and subsequently deposited in moraines is unlikely to have carried significant pre-exposure. The late-glacial to Holocene glaciers of the Southern Alps were relatively short and it is likely that the transit time of supraglacial rock debris from source to a moraine repository was a century or less (Schaefer et al., 2009; Balco, 2011; Putnam et al., 2012). To facilitate comparison with radiocarbon ages, all  $^{10}\text{Be}$  ages have been referenced to the year 1950 CE by subtracting 61 years from the calculated ages (all samples were collected in February 2011).

3.3. Glacier model application

Glacier reconstructions were made using a 2-dimensional energy, mass-balance, and ice-flow model (Plummer and Phillips, 2003) that has previously been applied to the last glacial maximum and subsequent recession of the Rakaia glacier (Putnam et al., 2013b; Rowan et al., 2013). Model parameterization used for the Rakaia glacier followed that employed by Rowan et al. (2013) and Putnam et al. (2013b), except for a smaller model domain used to consider only the upper Rakaia catchment upstream from Prospect Hill (Fig. 3). The use of this smaller model domain allowed a greater level of accuracy in the simulated glacier results compared to those determined over a larger domain. In particular, the smaller domain allows us to resolve with more confidence the change in ice

thickness resulting from small (<0.5 °C) variations in mean annual air temperature.

Model parameters and variables are given in Table 4 and briefly summarized here. The model domain is defined from the Land Information New Zealand (2011) 25-m digital elevation model (DEM), resampled to a 200-m grid resolution. Mean monthly air temperature and secondary climate variables (e.g. wind speed, cloudiness) are defined by values taken from automatic weather stations within 70 km of the Rakaia valley and reported in the New Zealand National Climate Database (CliFlo) (<http://cliflo.niwa.co.nz/>). Precipitation is defined using the National Institute of Water and Atmospheric Research (NIWA) 500-m gridded monthly data that are interpolated from 30 years of automatic weather station records (Tait et al., 2006).

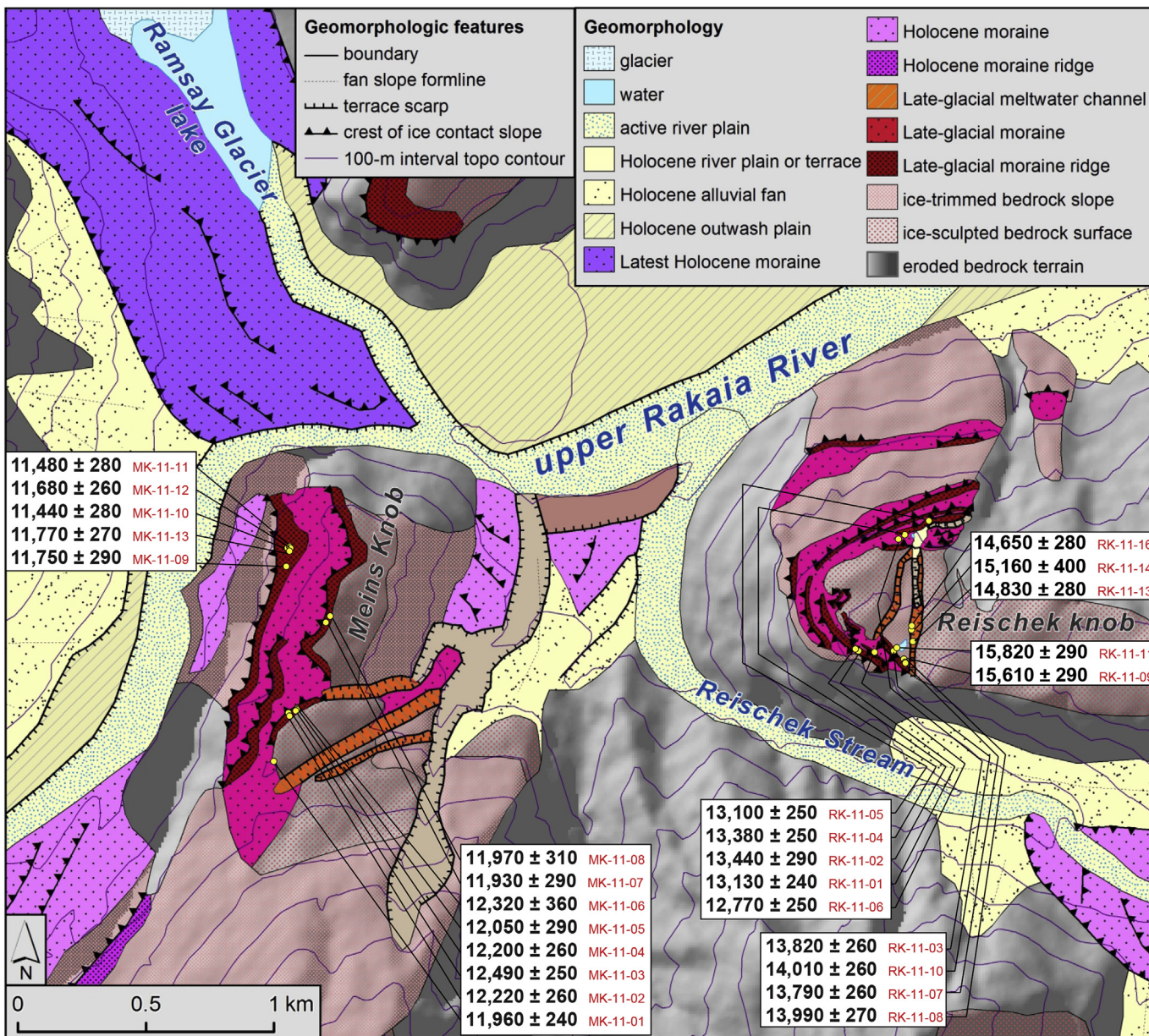


Fig. 4. Glacial geomorphologic map of a portion of the upper Rakaia valley showing the late-glacial moraines on Reischek knob and Meins Knob. Samples that record glacier recession during HS1 (RK-11-09, 11, 13, 14, and 16, Putnam et al., 2013b) are shown for clarity. Grayscale background image is a digital elevation model with relief highlighted by simulated illumination from the northwest. Ages are presented with 1σ internal uncertainty. Ages and sample numbers are connected by yellow lines to yellow dots that depict sample locations; several of these dots overlap at this map scale. (For interpretation of the references to colour in this figure legend, the reader is referred to the web version of this article.)

**Table 1**  
Rakaia valley surface-exposure sample details and  $^{10}\text{Be}$  data. Assumed density for all samples is  $2.7 \text{ g cm}^{-3}$

CAMS laboratory no.	Sample ID	Latitude (DD)	Longitude (DD)	Elevation (m a.s.l.)	Boulder Size (L × W × H) (cm)	Sample Thickness (cm)	Shielding correction	Quartzweight (g)	Carrier Added (mg $^9\text{Be}$ )	$^{10}\text{Be}/^9\text{Be} \pm 1\sigma$ ( $10^{-14}$ ) <sup>a</sup>	$[^{10}\text{Be}] \pm 1\sigma$ ( $10^4$ atoms $\times \text{g}^{-1}$ ) <sup>b</sup>	$^9\text{Be}$ Current ( $\mu\text{A}$ ) <sup>c</sup>	AMS Std <sup>d</sup> (Procedural blank number <sup>e</sup> )
<i>Reischek knob III</i>													
BE31678	RK-11-03	−43.291425	170.947971	1326	450 × 310 × 110	1.17	0.9759	15.5426	0.1894	19.47 ± 0.22	15.76 ± 0.18	7.9 (50.9)	07KNSTD (5,6)
BE31681	RK-11-07	−43.295769	170.948161	1448	155 × 120 × 50	2.08	0.9900	16.0868	0.1892	22.26 ± 0.24	17.40 ± 0.19	9.8 (63.5)	07KNSTD (5,6)
BE31682	RK-11-08	−43.295745	170.948151	1448	160 × 135 × 75	1.87	0.9888	15.4838	0.1890	21.77 ± 0.27	17.67 ± 0.22	9.4 (60.9)	07KNSTD (5,6)
BE31666	RK-11-10	−43.295343	170.947665	1443	170 × 55 × 165	2.66	0.9909	15.1403	0.1890	21.22 ± ± 0.23	17.57 ± 0.21	15.2 (98.1)	07KNSTD (1,2)
<i>Reischek knob IV</i>													
BE31662	RK-11-01	−43.295310	170.945962	1426	130 × 90 × 45	2.09	0.9939	15.0612	0.1890	19.66 ± 0.21	16.35 ± 0.19	19.9 (128.4)	07KNSTD (1,2)
BE31663	RK-11-02	−43.295231	170.945857	1425	170 × 110 × 75	2.30	0.9939	15.2938	0.1882	20.48 ± ± 0.32	16.70 ± 0.27	17.3 (112.2)	07KNSTD (1,2)
BE31664	RK-11-04	−43.291271	170.948296	1318	260 × 90 × 85	1.56	0.9752	15.5877	0.1888	18.69 ± 0.20	15.00 ± 0.18	17.7 (114.4)	07KNSTD (1,2)
BE31679	RK-11-05	−43.290820	170.949471	1300	165 × 150 × 95	1.08	0.9837	16.0919	0.1894	18.88 ± 0.21	14.77 ± 0.17	8.5 (54.9)	07KNSTD (5,6)
BE31680	RK-11-06	−43.295374	170.946695	1433	250 × 170 × 145	1.25	0.9891	16.0972	0.1894	20.47 ± 0.24	16.01 ± 0.20	8.9 (57.8)	07KNSTD (5,6)
<i>Meins Knob I</i>													
BE31670	MK-11-01	−43.298686	170.917643	1299	80 × 40 × 30	1.30	0.9902	20.5362	0.1896	22.14 ± 0.28	13.54 ± 0.19	14.8 (95.6)	07KNSTD (3,4)
BE31671	MK-11-02	−43.297112	170.918453	1266	275 × 225 × 90	1.05	0.9905	21.1158	0.1883	22.88 ± 0.35	13.52 ± 0.22	15.1 (97.7)	07KNSTD (3,4)
BE31672	MK-11-03	−43.297064	170.918452	1265	215 × 140 × 90	1.41	0.9856	19.4738	0.1899	21.21 ± 0.27	13.70 ± 0.19	16.0 (103.7)	07KNSTD (3,4)
BE31673	MK-11-04	−43.296919	170.918755	1261	205 × 95 × 70	1.68	0.9902	16.2426	0.1891	17.37 ± 0.27	13.38 ± 0.22	16.4 (106.3)	07KNSTD (3,4)
BE32801	MK-11-05	−43.296912	170.918798	1261	330 × 110 × 80	1.63	0.9889	15.8343	0.1899	16.69 ± 0.31	13.29 ± 0.25	16.4 (92.7)	07KNSTD (8)
BE32802	MK-11-06	−43.296894	170.918800	1260	210 × 80 × 60	2.17	0.9879	15.7988	0.1886	16.90 ± 0.42	13.40 ± 0.34	18.1 (102.5)	07KNSTD (8)
BE32803	MK-11-07	−43.293861	170.920314	1270	175 × 85 × 50	1.58	0.9908	15.6340	0.1901	16.30 ± 0.30	13.17 ± 0.25	17.2 (97.6)	07KNSTD (8)
BE32804	MK-11-08	−43.293649	170.920510	1274	120 × 110 × 70	2.59	0.9939	15.3610	0.1894	16.11 ± 0.33	13.20 ± 0.28	16.2 (91.5)	07KNSTD (8)
<i>Meins Knob II</i>													
BE32564	MK-11-09	−43.291841	170.918501	1154	145 × 100 × 40	2.35	0.9791	18.6204	0.1896	17.24 ± 0.32	11.64 ± 0.24	13.9 (85.7)	07KNSTD (7)
BE32805	MK-11-10	−43.291227	170.918613	1153	230 × 100 × 30	2.01	0.9837	15.4433	0.1891	14.02 ± 0.26	11.41 ± 0.22	15.2 (86.0)	07KNSTD (8)
BE32806	MK-11-11	−43.291148	170.918672	1152	370 × 220 × 145	2.38	0.9817	16.4010	0.1888	14.88 ± 0.28	11.38 ± 0.22	16.2 (91.7)	07KNSTD (8)
BE31674	MK-11-12	−43.291192	170.918701	1150	270 × 190 × 95	1.21	0.9790	13.6555	0.1888	12.76 ± 0.21	11.65 ± 0.21	15.7 (101.7)	07KNSTD (3,4)
BE31675	MK-11-13	−43.291328	170.918625	1151	310 × 230 × 135	1.34	0.9826	15.2240	0.1885	14.40 ± 0.24	11.78 ± 0.21	16.3 (105.1)	07KNSTD (3,4)

<sup>a</sup> Boron-corrected  $^{10}\text{Be}/^9\text{Be}$ . Ratios are not corrected for background  $^{10}\text{Be}$  detected in procedural blanks.

<sup>b</sup> Reported  $[^{10}\text{Be}]$  values have been corrected for background  $^{10}\text{Be}$  detected in procedural blanks.

<sup>c</sup>  $^9\text{Be}^{+3}$  measured after the accelerator. Reported currents are those measured during the first run of each sample. In parentheses is the ratio, given in percent, of each sample current compared with the average of all first-run AMS standard currents measured during the same CAMS session as the sample.

<sup>d</sup> AMS standard to which respective ratios and concentrations are referenced. Reported  $^{10}\text{Be}/^9\text{Be}$  ratio for 07KNSTD3110 is  $2.85 \times 10^{-12}$ .

<sup>e</sup> Blank number (left column in Table 3) of the respective procedural blank(s) used to correct each sample for background  $^{10}\text{Be}$ . Where two blank numbers appear the average of these was used to make the background correction.

**Table 2**  
 $^{10}\text{Be}$  surface-exposure ages (in yrs before 1950  $\pm 1\sigma$  internal error) from upper Rakaia valley landforms.

Sample ID	St age (yrs)	Lm age (yrs)
<b>Reischek knob outer moraine (RK-III)</b>		
RK-11-03	13,890 $\pm$ 260	13,820 $\pm$ 260
RK-11-07	13,870 $\pm$ 260	13,790 $\pm$ 260
RK-11-08	14,090 $\pm$ 280	13,990 $\pm$ 270
RK-11-10	14,100 $\pm$ 270	14,010 $\pm$ 260
<b>Reischek knob inner moraine (RK-IV)</b>		
RK-11-01	13,200 $\pm$ 250	13,130 $\pm$ 240
RK-11-02	13,510 $\pm$ 290	13,440 $\pm$ 290
RK-11-04	13,340 $\pm$ 250	13,280 $\pm$ 250
RK-11-05	13,160 $\pm$ 250	13,100 $\pm$ 250
RK-11-06	12,840 $\pm$ 250	12,770 $\pm$ 250
<b>Meins Knob outer moraine (MK-I)</b>		
MK-11-01	12,000 $\pm$ 240	11,960 $\pm$ 240
MK-11-02	12,260 $\pm$ 260	12,220 $\pm$ 260
MK-11-03	12,530 $\pm$ 250	12,490 $\pm$ 250
MK-11-04	12,240 $\pm$ 270	12,200 $\pm$ 260
MK-11-05	12,080 $\pm$ 290	12,050 $\pm$ 290
MK-11-06	12,360 $\pm$ 360	12,320 $\pm$ 360
MK-11-07	11,970 $\pm$ 290	11,930 $\pm$ 290
MK-11-08	12,000 $\pm$ 310	11,970 $\pm$ 310
<b>Meins Knob inner moraine (MK-II)</b>		
MK-11-09	11,770 $\pm$ 290	11,750 $\pm$ 290
MK-11-10	11,450 $\pm$ 280	11,440 $\pm$ 280
MK-11-11	11,490 $\pm$ 280	11,480 $\pm$ 280
MK-11-12	11,700 $\pm$ 260	11,680 $\pm$ 260
MK-11-13	11,800 $\pm$ 270	11,770 $\pm$ 270

The glacier model calculates surface energy balance across the model domain using the DEM topography and an estimate of solar position at 13,000 yrs ago to determine radiative fluxes. Ice flow is calculated using the shallow ice approximation and is by deformation only. The choice of ice flow parameters follows that used in previous studies of the Rakaia glacier (Putnam et al., 2013b; Rowan et al., 2013) and was designed to give the best fit of the simulated ice thickness to mapped terminal and lateral moraines in the Rakaia and Ashburton catchments. Following initial simulations for a given change in temperature, modeled glaciers were added to the DEM topography to recalculate mass balance iteratively across the simulated glacier surface, which had higher elevations for greater ice extents. Results from this ice-flow model were considered acceptable when the integrated mass balance (the difference between accumulation and ablation across the entire glacier) was within 4% of steady state (i.e. integrated balance =  $0 \pm 0.04$  m water equivalent per year). Glacier model simulations were run to simulate differences in temperature ( $\Delta T$ ) in increments of 0.25 °C

between  $-1.0$  and  $-2.25$  °C with respect to modern climate. For each component of the glacial sequence, we adopted the temperature depression, relative to modern, associated with the simulated ice margin that gave the best fit to the observed geomorphology.

#### 4. Chronology of late-glacial moraines in the upper Rakaia valley

We present 22  $^{10}\text{Be}$  surface-exposure ages of boulders on the moraine ridges of Reischek knob and Meins Knob (Table 2). All reported uncertainties on individual boulder ages include the one standard deviation analytical error (i.e.,  $1\sigma$ ) propagated with a 1.5% carrier concentration uncertainty as well as the procedural blank error. Moraine age uncertainties are reported as the  $1\sigma$  error on the arithmetic mean of the boulder population, with the production-rate (PR) uncertainty of 2.1% propagated in quadrature whenever we compare the moraine ages to independently dated records. The four boulders sampled from the Reischek knob III moraine range in age from 13,790  $\pm$  260 to 14,010  $\pm$  260 yrs with an arithmetic mean age of 13,900  $\pm$  120 yrs (13,900  $\pm$  310 yrs including PR uncertainty) (Fig. 5). Five sampled boulders from the Reischek knob IV moraine yield ages that range from 12,770  $\pm$  250 to 13,440  $\pm$  290 yrs, with an arithmetic mean age of 13,140  $\pm$  250 yrs (13,140  $\pm$  370 yrs including PR uncertainty). Eight boulders on the Meins Knob I moraine range in age from 11,930  $\pm$  290 to 12,490  $\pm$  250 yrs, and give an arithmetic mean age of 12,140  $\pm$  200 yrs (12,140  $\pm$  320 yrs including PR uncertainty). Exposure ages of five boulders embedded in the Meins Knob II moraine range from 11,440  $\pm$  280 to 11,770  $\pm$  270 yrs and afford an arithmetic mean age of 11,620  $\pm$  160 yrs (11,620  $\pm$  290 yrs including PR uncertainty).

Topographic profiling of moraines (Fig. 6) indicates that following the formation of moraines on Reischek knob at 13,900  $\pm$  120 and 13,140  $\pm$  250 yrs ago, the ice surface lowered by about 150 m relative to the Reischek knob IV moraine ridge. This allowed construction of the Meins Knob I moraine which culminated at 12,140  $\pm$  200 yrs ago. After a further thinning of  $\sim 100$  m, the glacier formed the Meins Knob II moraine at 11,620  $\pm$  160 yrs ago. The abandonment of that moraine implies further thinning of the glacier. Thus, the net thinning of glacier ice in the upper Rakaia valley between 13,140  $\pm$  250 and 11,620  $\pm$  160 yrs ago amounted to some 250 m (Fig. 6).

#### 5. Glacier-inferred paleoclimatic reconstruction

The upper Rakaia valley exhibits a complex hypsometry with a multitude of tributary valleys that present a challenge for accurate

**Table 3**  
 Blank data.

Blank No.	CAMS laboratory no.	Sample ID	Carrier Added (mg $^9\text{Be}$ )	$^{10}\text{Be}/^9\text{Be} \pm 1\sigma$ ( $10^{-16}$ ) <sup>a</sup>	$\text{N}^{10}\text{Be} \pm 1\sigma$ ( $10^3$ atoms) <sup>b</sup>	$^9\text{Be}$ current ( $\mu\text{A}$ ) <sup>c</sup>	AMS Std <sup>d</sup>
1	BE31668	Blank_1_2011Jun02	0.1883	7.83 $\pm$ 2.03	9.8 $\pm$ 2.6	19.4 (126%)	07KNSTD
2	BE31669	Blank_2_2011Jun02	0.1895	9.05 $\pm$ 1.71	11.5 $\pm$ 2.2	16.8 (109%)	07KNSTD
3	BE31676	Blank_1_2011Jun15	0.1891	11.1 $\pm$ 2.20	14.0 $\pm$ 2.8	14.3 (92%)	07KNSTD
4	BE31677	Blank_2_2011Jun15	0.1895	10.3 $\pm$ 2.17	13.0 $\pm$ 2.8	14.0 (91%)	07KNSTD
5	BE31686	Blank_1_2011Jun30	0.1895	3.74 $\pm$ 1.04	4.7 $\pm$ 1.3	18.9 (122%)	07KNSTD
6	BE31687	Blank_2_2011Jun30	0.1895	2.12 $\pm$ 0.815	2.7 $\pm$ 1.0	14.8 (95%)	07KNSTD
7	BE32562	Blank_2_2011_Oct10	0.1898	3.67 $\pm$ 3.37	4.7 $\pm$ 4.3	10.5 (65%)	07KNSTD
8	BE32800	Blank_3_2011Dec02	0.1896	0.846 $\pm$ 0.587	1.1 $\pm$ 0.7	16.5 (94%)	07KNSTD
				Arithmetic Mean $\pm 1\sigma$ :	7.69 $\pm$ 5.0		

<sup>a</sup> Boron-corrected  $^{10}\text{Be}/^9\text{Be}$ .

<sup>b</sup> Total  $^{10}\text{Be}$  contamination (in atoms) determined from each procedural blank.

<sup>c</sup>  $^9\text{Be}^{+3}$  measured after the accelerator. Reported currents are those measured during the first run of each sample. In parentheses is the ratio, given in percent, of each sample current compared with the average of all first-run AMS standard currents measured during the same CAMS session as the sample.

<sup>d</sup> AMS standards to which respective ratios and concentrations are referenced. Reported  $^{10}\text{Be}/^9\text{Be}$  ratio for 07KNSTD3110 is  $2.85 \times 10^{-12}$ .

**Table 4**  
Glacier model parameters.

Model domain description		Climatological parameters		Annual	Summer	Winter
Native horizontal resolution of LINZ DEM (m)	25	Monthly sea level temperature range (°C)		5.6–15.8	10.7–15.8	5.6–11.2
Vertical resolution of LINZ DEM (m)	1	Standard deviation of temperature (°C)		2.9	3.1	2.7
Cellsize of model domain (m)	200	Atmospheric lapse rate (°C km <sup>-1</sup> )		-6		
Model domain grid (number of cells)	208 × 211	Critical temperature for snowfall (°C)		2		
<b>Glaciological parameters</b>		NIWA rainfall maximum (mm)		8450		
High albedo	0.74	NIWA rainfall minimum (mm)		645		
Low albedo	0.21	NIWA rainfall mean (mm)		1602		
Maximum slope that can hold snow (degrees)	30	NIWA rainfall standard deviation (mm)		1129		
Slope increment for avalanching routine (degrees)	12	Wind speed (m s <sup>-1</sup> )		3.2	3.6	2.8
Minimum new snow for avalanching to occur (m)	0.1	Base wind speed elevation (m)		457		
		Multiplier for wind speed increase with elevation		0.0008		
Deformation constant (yr <sup>-1</sup> kPa <sup>-3</sup> )	2.1 × 10 <sup>-7</sup>	Cloudiness (fraction of sky covered)		0.7		
		Relative humidity		0.77	0.75	0.79
		Emissivity of snow		0.99		
		Emissivity of the surrounding terrain		0.94		
		Dimensionless transfer coefficient for snow		0.0015		
		Ground heat flux (W m <sup>-2</sup> )		0.1		
		<b>Climatological variables</b>				
		Linear change in MAAT (°C)		0–6.5		
		Precipitation multiplier		1–4		
		Period for solar angles calculation (ka)		13		

paleo-snowline reconstruction by traditional graphical methods. Hence we adopted the approach of glaciological numerical modeling to infer a temperature signal from our moraine record. We are aware that temperature is not the sole control on glacier mass balance, and recognize that large changes in precipitation amount can mimic the effects of small temperature changes (e.g. Anderson and Mackintosh, 2006; Rowan et al., 2014). However, we note that atmospheric temperature is observed to be the predominant control on recent glacier mass-balance changes in the central Southern Alps (Anderson et al., 2010; Rowan et al., 2014). The results of our modeling indicate that a mean annual air temperature of about 2 °C cooler than present values could have sustained the glacier margin at the position of the Reischek knob III and Reischek knob IV moraines (Fig. 7). The Meins Knob I and II moraines correspond to temperatures of ~1.25 °C and ~1.0 °C cooler than modern, respectively. Thus, the modeling indicates that the ~250 m lowering of the glacier surface in the upper Rakaia valley between 13,140 ± 250 and 11,620 ± 160 yrs ago can be accounted for by a mean annual air temperature increase of ~1 °C (Fig. 7).

## 6. Discussion

The glacial geomorphologic record of Rakaia valley reveals a pattern of glacier withdrawal through the last glacial termination in New Zealand (Fig. 8). Extensive recession occurred during HS 1 (~17,800–~14,700 yrs ago, Putnam et al., 2013b). Shortly thereafter, the Rakaia glacier paused, or alternatively may have resurged from a more retracted position, resulting in moraine construction on Reischek knob at ~13,900 and ~13,140 yrs ago under conditions of mean air temperature about 2.0 °C lower than today. This interval of moraine construction generally corresponds to the ACR originally registered in Antarctic ice cores. Further ice retreat between ~13,140 and ~11,620 yrs ago exposed Meins Knob during HS 0 (Younger Dryas), corresponding to an atmospheric warming of ~1.0 °C.

The late-glacial moraines on Reischek knob were constructed coevally with late-glacial moraines that we have dated elsewhere in the Southern Alps. The mid-Macaulay moraines in the Lake Tekapo catchment (“MM” in Fig. 2) date from ~13,300 yrs ago (Putnam et al., 2010b). In the Lake Pukaki catchment, the Pukaki glacier formed the Birch Hill moraines in two episodes at ~14,100 and

~13,000 yrs ago (Putnam et al., 2010b; “BH” in Fig. 2). In the Ben Ohau Range, a cirque glacier at the head of the Irishman Stream (Fig. 2) deposited the outermost late-glacial moraine at ~13,000 yrs ago (Kaplan et al., 2010; “IS” in Fig. 2). Also in the Ben Ohau Range, the most extensive late-glacial moraines in the two branches of Whale Stream range in age from ~15,400 to ~12,900 yrs ago (n = 6, east branch) and ~14,800 to ~13,400 yrs ago (n = 4, west branch) (Kaplan et al., 2013; “WS” in Fig. 2). An additional example of late-glacial ice resurgence is provided by wood with an age of ~13,000 yrs, incorporated within till at Canavans Knob, just inside the Waiho Loop moraine on the western side of the Southern Alps (Denton and Hendy, 1994; Putnam et al., 2010b; “WL” in Fig. 2). The general correspondence in timing of moraine construction among these sites indicates a widespread pause in the Southern Alps of warming and glacier recession, punctuated with intermittent glacier advances, between ~14,000 and ~13,000 years ago.

The subsequent HS 0 warming of ~1.0 °C in the Rakaia valley was only a quarter of the amount that occurred during HS 1 (Putnam et al., 2013b). Of the ~4 °C warming in the Rakaia valley during HS 1, 3.25 °C took place between ~17,900 and ~16,250 years ago (Putnam et al., 2013b, Table 5). The temperature increase of ~1 °C in the Rakaia valley during HS 0 is similar to the 0.65 °C warming estimated from an approximately contemporaneous snowline rise on the Irishman Stream cirque glacier, located 100 km to the southwest of the upper Rakaia valley (Kaplan et al., 2010; Doughty et al., 2013). Glacier recession during HS 0 also occurred at Whale Stream, situated near Irishman Stream, in response to an estimated net warming there of ~0.6 °C (Kaplan et al., 2013). These derived estimates agree within reported uncertainties, and indicate a moderate regional increase of temperature during HS 0.

Glacier records from southern South America yield a signature for the last glacial termination similar to that documented from the Southern Alps, implying an overall pan-Pacific pattern. Rapid warming and deglaciation in the Chilean Lake District between 39°S and 43°S began at ~17,800 yrs ago (Moreno et al., 2015). Glacier resurgence during the ACR at Lago Argentino (50°S) culminated at ~13,000 yrs ago with formation of the Puerto Bandera moraines, with subsequent recession during HS 0 interrupted by the formation of the Herminita moraines at ~12,200 yrs ago (Kaplan et al., 2011; Strelin et al., 2011). In Cordillera Darwin of Tierra del Fuego, extensive glacier recession occurred during the



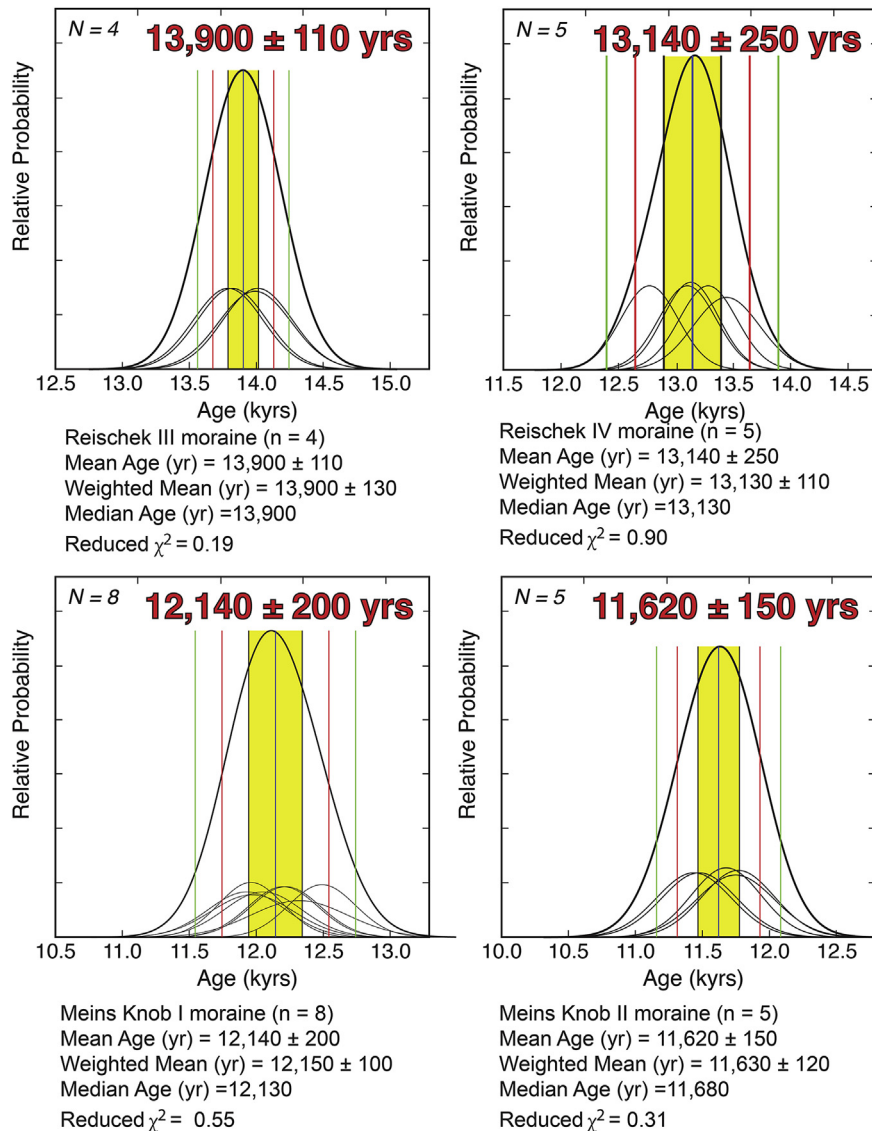


**Fig. 5.** Normal kernel density diagrams (Lowell, 1995; “camel plots” of Balco, 2011) of sample ages for each moraine ridge, expressed in thousands of years before 1950 CE (kyrs). Thin black lines are Gaussian curves for each sample. Thick black line is a Gaussian curve representing the sum of all samples from the respective moraine ridge. One-, two- and three- $\sigma$  confidence intervals of mean are shown as black, red, and green lines, respectively. The 1 $\sigma$  range discussed in the text is highlighted in yellow. Statistics for each plot appear below it. (For interpretation of the references to colour in this figure legend, the reader is referred to the web version of this article.)

first half of HS 1 (Hall et al., 2013). The ACR cool episode is also well documented in other paleoclimate proxies from the Pacific margin of southern South America, such as pollen- and chironomid-inferred temperatures from lacustrine sediment cores (Massaferro et al., 2009) and sea-surface temperature indicators from marine sediment cores (Lamy et al., 2004, 2007; Kaiser et al., 2005).

A detailed climate history for central West Antarctica has been derived from a combination of ice accumulation, isotopic and borehole temperature records in the WAIS Divide ice core (WAIS Divide Project Members, 2013; Buizert et al., 2015; Cuffey et al., 2016; see Fig. 8). These West Antarctic records indicate a sustained rise in accumulation rate and atmospheric temperature through HS 1, followed by a general plateau or decrease in accumulation and temperature during the ACR, and then further rise towards Holocene conditions. The similarity to the Rakaia valley glacier-climate reconstruction record is striking, where there was sustained warming during HS 1, a plateau in overall warming during the ACR with episodes of late-glacial moraine formation, followed by progressive slight rise in temperature through HS

0 (Fig. 8).

An important element of the Rakaia valley/West Antarctica comparison is the correlation between the glacier-inferred temperature reconstruction from the Rakaia valley and the accumulation rates inferred from the WAIS Divide ice core. Atmospheric temperature exerts a first-order control on moisture delivered to the Antarctic interior and precipitated as snow, with a secondary control being the strength of the Antarctic circumpolar vortex (Bromwich, 1988; Frieler et al., 2015). Accumulation rates at WAIS Divide increased sharply at ~18,000 yrs ago and achieved near-interglacial levels by ~15,500 yrs ago, all during HS 1. Snow accumulation rate at the WAIS Divide core site nearly doubled during HS 1 (WAIS Divide Project Members, 2013). This record of Antarctic snow accumulation suggests that rapid warming of Antarctic atmospheric temperature was basically complete by the end of HS 1. We infer from the general similarity between Rakaia glacier recession and the jump in Antarctic snow accumulation during HS 1 that rapid warming to near-interglacial conditions commenced in both places at about the same time, further extending the footprint

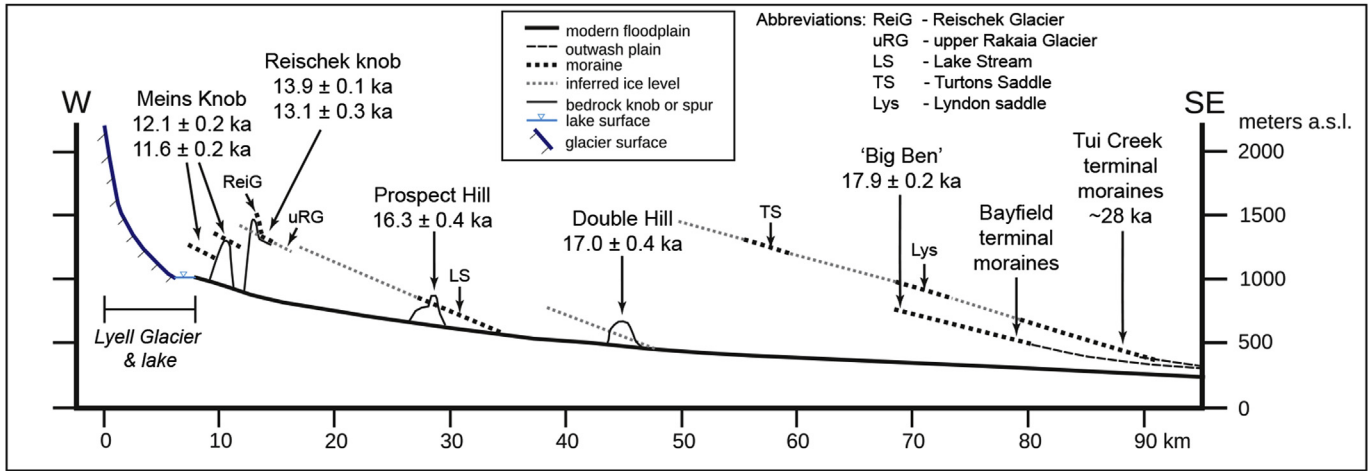


Fig. 6. Profile of the Rakaia valley. Mapped moraine elevations are projected perpendicularly onto the profile line (see Fig. 3). Vertical exaggeration is approximately 11:1.

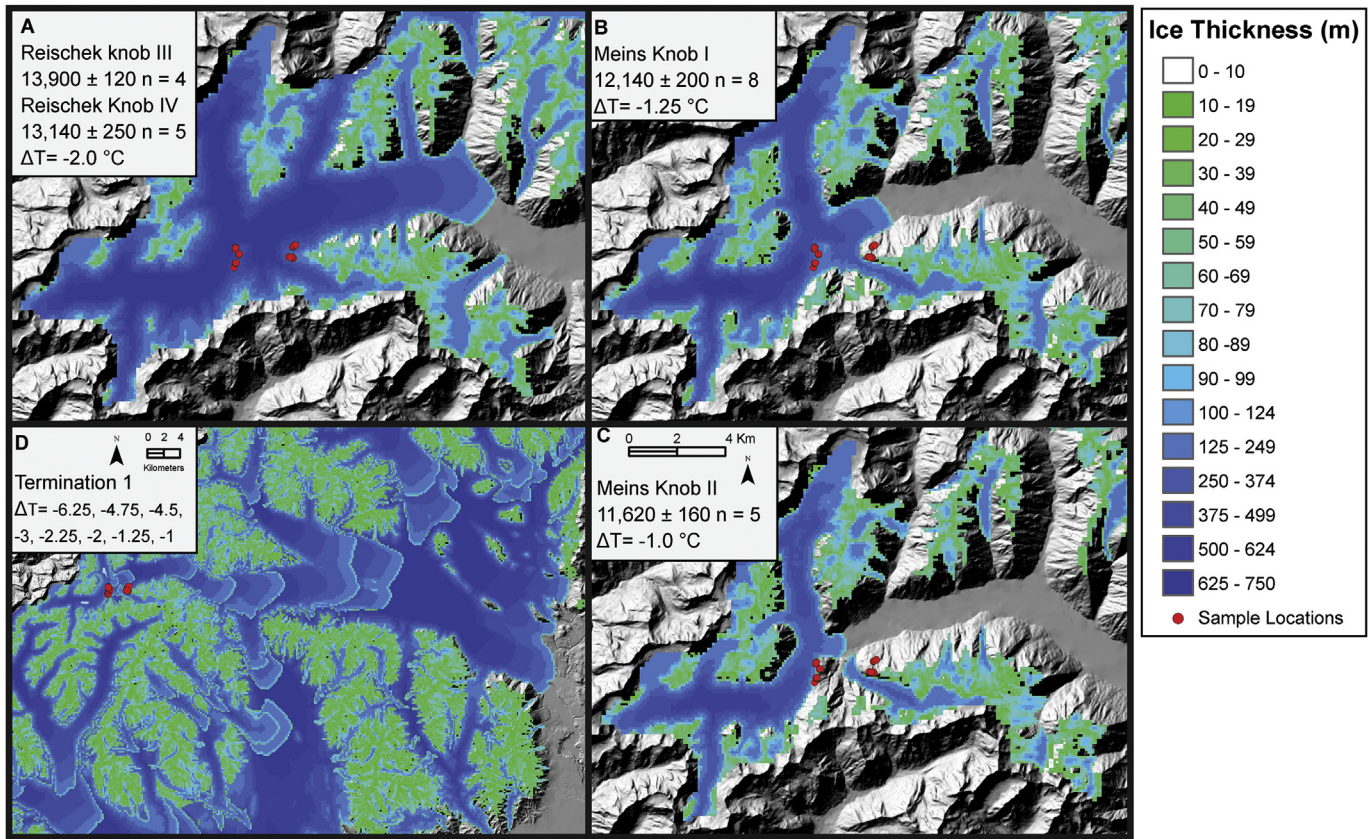


Fig. 7. Glacier model results; a) Reischek knob III and IV,  $\Delta T = -2.0\text{ }^{\circ}\text{C}$ ; b) Meins Knob I,  $\Delta T = -1.25\text{ }^{\circ}\text{C}$ ; c) Meins Knob II,  $\Delta T = -1.0\text{ }^{\circ}\text{C}$ . Distance scale in c) also applies to a) and b). d) stacked results for HS 1 through HS 0, smaller scale. Color scale represents ice thickness, where green shades show ice 10–50 m thick. Ice less than 10 m thick is not shown. Sample locations are shown by red circles, many of which overlap on this figure. (For interpretation of the references to colour in this figure legend, the reader is referred to the web version of this article.)

of this remarkable warming event from 44°S to the deep interior of West Antarctica. This scenario is generally supported by isotope-derived temperatures from the WAIS Divide ice core (Cuffey et al., 2016), particularly on the millennial time scale. However, we find the best match when comparing glacier-derived temperatures in the Southern Alps with WAIS Divide accumulation rates. Several late-glacial century-scale reductions in WAIS accumulation are coeval with glacier resurgence in the Rakaia valley, but the WAIS

temperature reconstruction co-registers only one of the century-scale accumulation dips, at ~16,000 yrs ago.

### 7. Conclusions

We used  $^{10}\text{Be}$  surface-exposure dating combined with a glaciological model of the upper Rakaia glacier to infer late-glacial temperature change in the Southern Alps of New Zealand. The

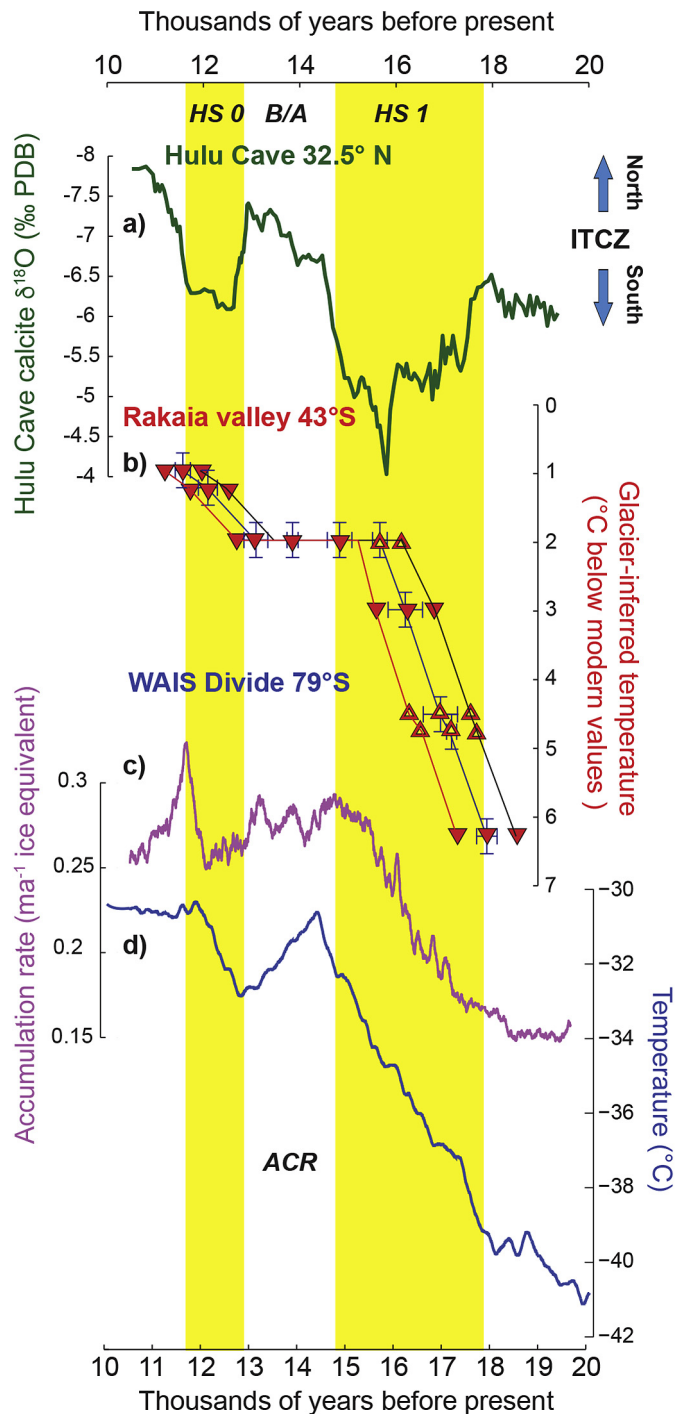


**Fig. 8.** a) Hulu Cave oxygen-isotope record (Wang et al., 2001); HS is Heinrich Stadial and B/A is Bølling/Allerød. b) Rakaia valley glacier-inferred temperature record (this study; Putnam et al., 2013b). Ages are plotted as the mean  $\pm$  one standard deviation of all samples from each moraine. Downward-pointing, solid red triangles represent samples from boulders embedded in moraine ridges, while upward-pointing, open triangles represent boulder samples resting on ice-sculpted bedrock surfaces. Red and black curves show the minimum and maximum ages possible for the chronology when production rate uncertainty (which shifts the ages in concert) is considered. Temperature uncertainty inferred from glacier modeling is  $\pm 0.25$  °C. c) Snow accumulation at the WAIS Divide ice core site (WAIS Divide Project Members, 2013). d) Borehole-calibrated temperature from the WAIS Divide ice core site (Cuffey et al., 2016). (For interpretation of the references to colour in this figure legend, the reader is referred to the web version of this article.)

upper Rakaia glacier built moraines at  $\sim 13,900$  and  $\sim 13,140$  yrs ago, during the ACR, in response to temperatures some 2 °C cooler than

**Table 5**

Glacier-inferred temperature chronology. Ext. uncertainty includes production-rate error.

Glacier position	Mean age $\pm$ 1s (yrs)	Ext. uncertainty (yrs)	$\Delta T$ (°C below modern)
Big Ben	17940 $\pm$ 210	431	-6.25
Lake Coleridge	17170 $\pm$ 100	374	-4.75
Double Hill	16970 $\pm$ 360	507	-4.50
Prospect Hill	16250 $\pm$ 360	496	-3.00
Reischek knob-I	15720 $\pm$ 150	363	-2.00
Reischek knob-II	14880 $\pm$ 260	407	-2.00
Reischek knob-III	13900 $\pm$ 110	312	-2.00
Reischek knob-IV	13140 $\pm$ 250	372	-2.00
Meins Knob I	12140 $\pm$ 200	324	-1.25
Meins Knob II	11620 $\pm$ 160	292	-1.00

modern values. Subsequent glacier recession during HS 0 was driven by net warming of  $\sim 1$  °C between  $\sim 13,140$  and  $\sim 11,620$  yrs ago. Our results provide a deglacial atmospheric temperature signature in New Zealand mirroring that registered over the West Antarctic Ice Sheet. Taken together with information from South America, these results imply that southern mid-to-high latitudes experienced a remarkable warming during HS 1 that brought the climate from glacial to near-interglacial temperatures. This net warming trend subsided around  $\sim 14,000$  yrs ago, with episodes of glacier margin expansion or stillstand, superimposed on a subtle net warming trend into the Holocene. Any explanation for last glacial termination must explain a unified climatic signal extending from the Southern Alps of New Zealand to the interior of West Antarctica.

#### Acknowledgements

This work was supported by the Comer Science and Education Foundation, the Quesada Family Foundation, and the National Science Foundation (NSF grant EAR-1102782). T.N.B. Koffman was supported by U.S. National Science Foundation Graduate Research Fellowship (grant number DGE-1144205) while conducting this research. D.J.A. Barrell was supported by funding from the New Zealand Government through the GNS Science research program “Global change through time”. A.E. Putnam was supported by funding from the Comer Science and Education Foundation and the Lenfest Foundation. We thank A. and T. Hutchinson of Double Hill Station for their hospitality and logistical support. We thank the Department of Conservation, Te Papa Atawhai and Te Rūnanga o Ngāi Tahu for permission to access and to sample the moraines of the upper Rakaia valley. The authors thank two anonymous reviewers for thoughtful suggestions that improved the manuscript. This paper is LDEO contribution no. 8123.

#### References

- Anderson, B., Mackintosh, A., 2006. Temperature change is the major driver of late glacial and Holocene glacier fluctuations in New Zealand. *Geology* 34, 121–124.
- Anderson, B., Mackintosh, A., Stumm, D., George, L., Kerr, T., Winter-Billington, A., Fitzsimons, S., 2010. Climate sensitivity of a high-precipitation glacier in New Zealand. *J. Glaciol.* 56, 114–128.
- Balco, G., Stone, J.O., Lifton, N.A., Dunai, T.J., 2008. A complete and easily accessible means of calculating surface exposure ages or erosion rates from  $^{10}\text{Be}$  and  $^{26}\text{Al}$  measurements. *Quat. Geochronol.* 4, 93–107.
- Balco, G., 2011. Contributions and unrealized potential contributions of cosmogenic nuclide exposure dating to glacier chronology, 1990–2010. *Quat. Sci. Rev.* 30, 3–27.
- Barrell, D.J.A., 2011. Quaternary Glaciers of New Zealand. In: Ehlers, J., Gibbard, P.L., Hughes, P.D. (Eds.), *Quaternary Glaciations - Extent and Chronology, Part IV - a Closer Look*. Elsevier, Amsterdam, pp. 1047–1064.
- Barrell, D.J.A., Andersen, B.G., Denton, G.H., 2011. Glacial geomorphology of the central South Island, New Zealand. *GNS Sci. Monogr.* 27, 81. GNS Science, Low. Hutt. Map (5 sheets).

- Bostock, H.C., Hayward, B.W., Neil, H.L., Sabaa, A.T., Scott, G.H., 2015. Changes in the position of the Subtropical Front south of New Zealand since the last glacial period. *Paleoceanography* 30, 824–844.
- Bromwich, D.H., 1988. Snowfall in high southern latitudes. *Rev. Geophys.* 26, 149–168.
- Brook, E.J., White, J.W.C., Schilla, A.S.M., Bender, M.L., Barnett, B., Severinghaus, J.P., Taylor, K.C., Alley, R.B., Steig, E.J., 2005. Timing of millennial-scale climate change at Siple Dome, West Antarctica, during the Last Glacial period. *Quat. Sci. Rev.* 24, 1333–1343.
- Buizert, C., Cuffey, K.M., Severinghaus, J.P., Baggenstos, D., Fudge, T.J., Steig, E.J., Markle, B.R., Winstrup, M., Rhodes, R.H., Brook, E.J., Sowers, T.A., Clow, G.D., Cheng, H., Edwards, R.L., Sigl, M., McConnell, J.R., Taylor, K.C., 2015. The WAIS Divide deep ice core WD2014 chronology – Part 1: methane synchronization (68–31 ka BP) and the gas age–ice age difference. *Clim. Past* 11, 153–173.
- Burrows, C.J., Russell, J.B., 1975. Moraines of the upper rakaia valley. *J. R. Soc. N. Z.* 5, 463–477.
- Carter, L., Garlick, R.D., Sutton, P., Chiswell, S., Oien, N.A., Stanton, B.R., 1998. Ocean circulation New Zealand. NIWA Chart Misc. Ser. 76. NIWA, Wellington.
- Cox, S.C., Barrell, D.J.A., 2007. Geology of the Aoraki Area, vol 1. Institute of Geological and Nuclear Sciences, 250,000 Geological Map 15. GNS Science, Lower Hutt. 1 sheet and 71 pp.
- Cuffey, K.M., Clow, G.D., Steig, E.J., Buizert, C., Fudge, T.J., Koutnik, M., Waddington, E.D., Alley, R.B., Severinghaus, J.P., 2016. Deglacial temperature history of West Antarctica. *Proc. Natl. Acad. Sci. U.S.A.* 113, 14,249–14,254.
- De Deckker, P., Moros, M., Perner, K., Jansen, E., 2012. Influence of the tropics and southern westerlies on glacial interhemispheric asymmetry. *Nat. Geosci.* 5, 266–269.
- Denton, G.H., Hendy, C.H., 1994. Younger Dryas age advance of Franz Josef glacier in the Southern Alps of New Zealand. *Science* 264, 1434–1437.
- Ditchburn, R.G., Whitehead, N.E., 1994. The Separation of  $^{10}\text{Be}$  from Silicates. 3<sup>rd</sup> Workshop of the South Pacific. Environmental Radioactivity Association, pp. 4–7.
- Doughty, A.M., Anderson, B.M., Mackintosh, A.N., Kaplan, M.R., Vandergoes, M.J., Barrell, D.J.A., Denton, G.H., Schaefer, J.M., Chinn, T.J.H., Putnam, A.E., 2013. Evaluation of lateglacial temperatures in the Southern Alps of New Zealand based on glacier modelling at Irishman Stream, Ben Ohau Range. *Quat. Sci. Rev.* 74, 160–169.
- Frieler, K., Clark, P.U., He, F., Buizert, C., Reese, R., Ligtenberg, S.R.M., van den Broeke, M.R., Winkelmann, R., Levermann, A., 2015. Consistent evidence of increasing Antarctic accumulation with warming. *Nat. Clim. Change* 5, 348–352.
- Golledge, N.R., Mackintosh, A.N., Anderson, B.M., Buckley, K.M., Doughty, A.M., Barrell, D.J.A., Denton, G.H., Vandergoes, M.J., Andersen, B.G., Schaefer, J.M., 2012. Last glacial maximum climate in New Zealand inferred from a modelled Southern Alps icefield. *Quat. Sci. Rev.* 46, 30–45.
- Hall, B.L., Porter, C.T., Denton, G.H., Lowell, T.V., Bromley, G.R.M., 2013. Extensive recession of cordillera Darwin glaciers in southernmost South America during Heinrich Stadial 1. *Quat. Sci. Rev.* 62, 49–55.
- Kaiser, J., Lamy, F., Hebbeln, D., 2005. A 70-kyr sea surface temperature record off southern Chile (Ocean Drilling Program Site 1233). *Paleoceanography* 20, PA4009.
- Kaplan, M.R., Schaefer, J.M., Denton, G.H., Barrell, D.J.A., Chinn, T.J.H., Putnam, A.E., Andersen, B.G., Finkel, R.C., Schwartz, R., Doughty, A.M., 2010. Glacier retreat in New Zealand during the Younger Dryas stadial. *Nature* 467, 194–197.
- Kaplan, M.R., Strelin, J.A., Schaefer, J.M., Denton, G.H., Finkel, R.C., Schwartz, R., Putnam, A.E., Vandergoes, M.J., Goehring, B.M., Travis, S.G., 2011. In-situ cosmogenic  $^{10}\text{Be}$  production rate at Lago Argentino, Patagonia: implications for late-glacial climate chronology. *Earth and Planet. Sci. Lett.* vol 309, 21–32.
- Kaplan, M.R., Schaefer, J.M., Denton, G.H., Doughty, A.M., Barrell, D.J.A., Chinn, T.J.H., Putnam, A.E., Andersen, B.G., Mackintosh, A., Finkel, R.C., Schwartz, R., Anderson, B., 2013. The anatomy of long-term warming since 15 kyr ago in New Zealand based on net glacier snowline rise. *Geology* 41, 887–890.
- Kelly, M.A., 2003. The Late Würmian Age in the Western Swiss Alps – Last Glacial Maximum Ice-Surface Reconstruction and  $^{10}\text{Be}$  Dating Of Late-Glacial Features. Ph.D. dissertation. University of Bern, p. 105.
- Lal, D., 1991. Cosmic-ray labeling of erosion surfaces: in situ nuclide production rates and erosion models. *Earth Planet. Sci. Lett.* 104, 424–439.
- Lamy, F., Kaiser, J., Arz, H., Ninnemann, U., Hebbeln, D., 2004. Antarctic timing of surface water changes off Chile and Patagonian ice sheet response. *Science* 304, 1959–1962.
- Lamy, F., Kaiser, J., Arz, H., Ninnemann, U., Hebbeln, D., Timm, O., Timmermann, A., Toggweiler, J., 2007. Modulation of the bipolar seesaw in the southeast Pacific during termination 1. *Earth Planet. Sci. Lett.* 259, 400–413.
- Lifton, N., Smart, B., Shea, M., 2008. Scaling time-integrated in situ cosmogenic nuclide production rates using a continuous geomagnetic model. *Earth Planet. Sci. Lett.* 268, 190–201.
- Lowell, T.V., 1995. The application of radiocarbon age estimates to the dating of glacial sequences: an example from the Miami Sublobe, Ohio, USA. *Quat. Sci. Rev.* 14, 85–99.
- Massaferro, J.L., Moreno, P.I., Denton, G.H., Vandergoes, M., Dieffenbacher-Krall, A., 2009. Chironomid and pollen evidence for climate fluctuations during the last glacial termination in NW Patagonia. *Quat. Sci. Rev.* 28, 517–525.
- Moreno, P.I., Denton, G.H., Moreno, H., Lowell, T.V., Putnam, A.E., Kaplan, M.R., 2015. Radiocarbon chronology of the last glacial maximum and its termination in northwestern Patagonia. *Quat. Sci. Rev.* 122, 233–249.
- Newnham, R.M., Vandergoes, M.J., Sikes, E., Carter, L., Wilmshurst, J.M., Lowe, D.J., McGlone, M.S., Sandiford, A., 2012. Does the bipolar seesaw extend to the terrestrial southern mid-latitudes? *Quat. Sci. Rev.* 36, 214–222.
- Oerlemans, J., 1997. Climate sensitivity of Franz Josef Glacier, New Zealand, as revealed by numerical modelling. *Arct. Alp. Res.* 29, 233–239.
- Oerlemans, J., 2005. Extracting a climate signal from 169 glacier records. *Science* 308, 675–677.
- Orsi, A.H., Whitworth, T., Nowlin, W.D., 1995. On the meridional extent and fronts of the Antarctic circumpolar current. *Deep-Sea Res.* 42, 64–673.
- Pedro, J.B., van Ommen, T.D., Rasmussen, S.O., Morgan, V.I., Chappellaz, J., Moy, A.D., Masson-Delmotte, V., Delmotte, M., 2011. The last deglaciation: timing the bipolar seesaw. *Clim. Past* 7, 671–683.
- Pedro, J.B., Bostock, H.C., Bitz, C.M., He, F., Vandergoes, M.J., Steig, E.J., Chase, B.M., Krause, C.E., Rasmussen, S.O., Markle, B.R., Cortese, G., 2016. The spatial extent and dynamics of the Antarctic Cold Reversal. *Nat. Geosci.* 9, 51–56.
- Plummer, M.A., Phillips, F.M., 2003. A 2-D numerical model of snow/ice energy balance and ice flow for paleoclimatic interpretation of glacial geomorphic features. *Quat. Sci. Rev.* 22, 1389–1406.
- Purdie, H., Mackintosh, A., Lawson, W., Anderson, B., Morgenstern, U., Chinn, T., Mayewski, P., 2011. Interannual variability in net accumulation on Tasman Glacier and its relationship with climate. *Glob. Planet. Change* 77, 142–152.
- Putnam, A.E., Schaefer, J.M., Barrell, D.J.A., Vandergoes, M., Denton, G.H., Kaplan, M.R., Schwartz, R., Finkel, R.C., Goehring, B.M., Kelley, S.E., 2010a. In situ cosmogenic  $^{10}\text{Be}$  production-rate calibration from the Southern Alps, New Zealand. *Quat. Geochronol.* 5, 392–409.
- Putnam, A.E., Denton, G.H., Barrell, D.J.A., Andersen, B.G., Finkel, R., Schwartz, R., Doughty, A.M., Kaplan, M., Schlüchter, C., 2010b. Glacier advance in southern middle latitudes during the Antarctic Cold Reversal. *Nat. Geosci.* 3, 700–704.
- Putnam, A.E., Schaefer, J.M., Denton, G.H., Barrell, D.J.A., Finkel, R.C., Andersen, B.G., Schwartz, R., Chinn, T.J.H., Doughty, A.M., 2012. Regional climate control of glaciers in New Zealand and Europe during the pre-industrial Holocene. *Nat. Geosci.* 5, 627–630.
- Putnam, A.E., Schaefer, J.M., Denton, G.H., Barrell, D.J.A., Birkel, S.D., Andersen, B.G., Kaplan, M.R., Finkel, R.C., Schwartz, R., Doughty, A.M., 2013a. The Last Glacial Maximum at 44°S documented by a  $^{10}\text{Be}$  moraine chronology at Lake Ohau, Southern Alps of New Zealand. *Quat. Sci. Rev.* 62, 114–141.
- Putnam, A.E., Schaefer, J.M., Denton, G.H., Barrell, D.J.A., Andersen, B.G., Koffman, T.N.B., Rowan, A.V., et al., 2013b. Warming and glacier recession in the Rakaia valley, Southern Alps of New Zealand, during Heinrich Stadial 1. *Earth Planet. Sci. Lett.* 382, 98–110.
- Rasmussen, S.O., Andersen, K.K., Svensson, A.M., Steffensen, J.P., Vinther, B.M., Clausen, H.B., Siggaard-Andersen, M.-L., Johnsen, S.J., Larsen, L.B., Dahl-Jensen, D., Bigler, M., Röthlisberger, R., Fischer, H., Goto-Azuma, K., Hansson, M.E., Ruth, U., 2006. A new Greenland ice core chronology for the last glacial termination. *J. Geophys. Res.* 111, D06102.
- Rood, D.H., Hall, S., Guilderson, T.P., Finkel, R.C., Brown, T.A., 2010. Challenges and opportunities in high-precision Be-10 measurements at CAMS. *Nucl. Instrum. Methods B Beam Interact. Mater. Atoms* 268 (7–8), 730–732.
- Rood, D.H., Brown, T.A., Finkel, R.C., Guilderson, T.P., 2013. Poisson and non-Poisson uncertainty estimations of  $^{10}\text{Be}/\beta\text{Be}$  measurements at LLNL–CAMS. *Nucl. Instrum. Methods B Beam Interact. Mater. Atoms* 294, 426–429.
- Rowan, A.V., Plummer, M.A., Brocklehurst, S.H., Jones, M.A., Schultz, D.M., 2013. Drainage capture and discharge variations driven by glaciation in the Southern Alps, New Zealand. *Geology* 41, 199–202.
- Rowan, A.V., Brocklehurst, S.H., Schultz, D.M., Plummer, M.A., Anderson, L.S., Glasser, N.F., 2014. Late Quaternary glacier sensitivity to temperature and precipitation distribution in the Southern Alps of New Zealand. *J. Geophys. Res.* 119, 1064–1081.
- Schaefer, J.M., Denton, G.H., Kaplan, M., Putnam, A., Finkel, R.C., Barrell, D.J.A., Andersen, B.G., Schwartz, R., Mackintosh, A., Chinn, T., Schlüchter, C., 2009. High-frequency Holocene glacier fluctuations in New Zealand differ from the northern signature. *Science* 324, 622–625.
- Shulmeister, J., Fink, D., Hyatt, D., Thackray, G., Rother, H., 2010. Cosmogenic  $^{10}\text{Be}$  and  $^{26}\text{Al}$  exposure ages of moraines in the Rakaia Valley, New Zealand and the nature of the last termination in New Zealand glacial systems. *Earth Planet. Sci. Lett.* 297, 558–566.
- Stenni, B., et al., 2011. Expression of the bipolar see-saw in Antarctic climate records during the last deglaciation. *Nat. Geosci.* 4, 46–49.
- Stone, J.O., 2000. Air pressure and cosmogenic isotope production. *J. Geophys. Res.* 105, 23753–23759.
- Strelin, J.A., Denton, G.H., Vandergoes, M.J., Ninnemann, U.S., Putnam, A.E., 2011. Radiocarbon chronology of the late-glacial Puerto Bandera moraines, Southern Patagonian icefield, Argentina. *Quat. Sci. Rev.* 30, 2551–2569.
- Tait, A., Henderson, R., Turner, R., Zheng, X., 2006. Thin plate smoothing spline interpolation of daily rainfall for New Zealand using a climatological rainfall surface. *Int. J. Climatol.* 26, 2097–2115.
- WAIS Divide Project Members, 2013. Onset of deglacial warming in West Antarctica driven by local orbital forcing. *Nature* 500, 440–444.
- Wang, Y.J., Cheng, H., Edwards, R.L., An, Z.S., Wu, J.Y., Shen, C.-C., Dorale, J.A., 2001. A high-resolution absolute-dated late Pleistocene monsoon record from Hulu Cave, China. *Science* 294, 2345–2348.